Multiscale Amplitude-Modulation Frequency-Modulation (AM–FM) Texture Analysis of Ultrasound Images of the Intima and Media Layers of the Carotid Artery

C. P. Loizou, *Member, IEEE*, V. Murray, *Member, IEEE*, M. S. Pattichis, *Senior Member, IEEE*, M. Pantziaris, and C. S. Pattichis, *Senior Member, IEEE*

***Abstract*—The intima-media thickness (IMT) of the common carotid artery (CCA) is widely used as an early indicator of cardiovascular disease (CVD). Clinically, there is strong interest in identifying how the composition and texture of the media layer (ML) can be associated with the risk of stroke. In this study, we use 2-D amplitude-modulation frequency-modulation (AM–FM) analysis of the intima-media complex (IMC), the ML, and intima layer (IL) of the CCA to detect texture changes as a function of age and sex. The study was performed on 100 ultrasound images acquired from asymptomatic subjects at risk of atherosclerosis. To investigate texture variations associated with age, we separated them into three age groups: 1) patients younger than 50; 2) patients aged between 50 and 60 years old; and 3) patients over 60 years old. We also separated the patients by sex. The IMC, ML, and IL were segmented manually by a neurovascular expert and also by a snake-based segmentation system. To reject strong edge artifacts, we prefilter with an AM–FM filterbank that is centered along the horizontal frequency axis (parallel to the long axis of the IMC, ML, and IL), while removing the low-pass filter estimates and frequency bands with large, vertical frequency components. To investigate significant texture changes, we extract the instantaneous amplitude (IA) and the magnitude of the instantaneous frequency (IF) over each layer component, for low-, medium-, and high-frequency AM–FM components. We detected significant texture differences between the higher risk age group of $>$60 years versus the lower risk age group of $<$50 and the 50–60 group. In particular, between the $<$50 and $>$60 groups, we found significant differences in the medium-scale IA extracted from the IMC. Between the $>$60 and the 50–60 groups, we found significant texture changes in the low-scale IA and high-scale IF magnitude extracted from the IMC, and the low-scale IA extracted from the IL. Also, we noted that the IA for the ML showed significant differences between males and females for all age groups. The AM–FM features provide complimentary information to classical texture analysis features like the gray-scale median, contrast, and coarseness. These findings provide evidence that AM–FM texture features can be associated with the progression of cardiovascular risk for disease and the risk of stroke with age. However, a larger scale study is needed to establish the application in clinical practice.**

***Index Terms*—Amplitude-modulation frequency-modulation (AM–FM), carotid, intima-media thickness (IMT), texture analysis.**

Manuscript received March 3, 2010; revised August 9, 2010; accepted September 22, 2010. Date of publication September 30, 2010; date of current version March 4, 2011.

C. P. Loizou is with the Department of Computer Science, School of Sciences, Intercollege, Limassol 3507, Cyprus, and also with the Institute of Neurology and Genetics, 1683 Nicosia, Cyprus (e-mail: loizou.c@lim.intercollege.ac.cy; panloicy@logosnet.cy.net).

V. Murray and M. S. Pattichis are with the Department of Electrical and Computer Engineering, University of New Mexico, Albuquerque, NM 87131 USA (e-mail: vmurray@ieee.org; pattichis@ece.unm.edu).

M. Pantziaris is with the Cyprus Institute of Neurology and Genetics, Nicosia 1683, Cyprus (e-mail: pantzari@cing.ac.cy).

C. S. Pattichis is with the Department of Computer Science, University of Cyprus, Nicosia 1678, Cyprus (e-mail: pattichi@ucy.ac.cy).

Color versions of one or more of the figures in this paper are available online at http://ieeexplore.ieee.org.

Digital Object Identifier 10.1109/TITB.2010.2081995

NOMENCLATURE

The following abbreviations were used in this study:

AM–FM:	Amplitude-modulation frequency-modulation.
$a_n(x,y)$:	n_{th} Instantaneous amplitude (IA) function.
CCA:	Common carotid artery.
CVD:	Cardiovascular disease.
DCA:	Dominant component analysis.
DV:	Difference variance.
GSM:	Gray scale median.
HIA:	High instantaneous amplitude.
$H_{2\text{-D}}$:	2-D Hilbert transform.
HIF:	High instantaneous frequency.
$\nabla\phi_n\,(x,y)$:	n_{th}Instantaneous frequency (IF) function.
IW:	Instantaneous wavelengths.
IMCGSM:	Intima media complex gray scale median.
IL GSM:	Intima layer gray scale median.
IL:	intima layer.
IMC:	Intima-media complex.
IMT:	Intima-media thickness.
IA:	Instantaneous amplitude.
IF:	Instantaneous frequency.
|IF|:	Instantaneous frequency magnitude.
IQR:	inter-quartile range.
ILT:	Intima layer thickness.
IM:	Intima media.
$I(x,y)$:	Acquired ultrasound image.
LPF:	Low-pass filter.
LIA:	Low scale instantaneous amplitude.
LIF:	Low scale instantaneous frequency.

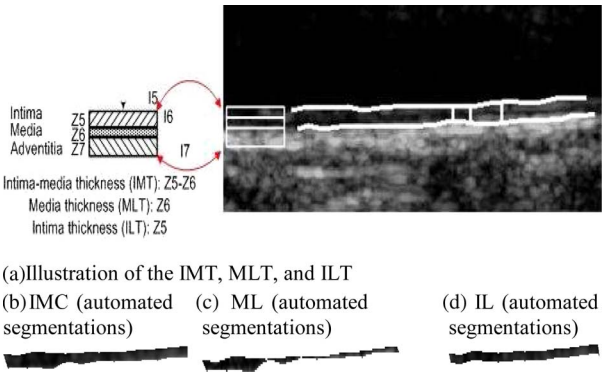

Fig. 1. Anatomical locations of ultrasound image components for atherosclerosis. The IMC in b), ML in c), and the IL in d), have been extracted using automated segmentation as described in [5], [7], and [25]. The ML is defined as the layer (band) between the IM and the media–adventitia interface (band Z6). CCA ultrasound indicating the location of the IMC at the far wall, segmented IMC (IMT = 0.79 mm, left column), segmented ML (MLT = 0.32 mm, middle column), and segmented IL (ILT = 0.47 mm, right column).

MLT:	Media layer thickness.
MIA:	Medium scale instantaneous amplitude.
MIF:	Medium scale instantaneous frequency.
ML:	Media layer.
MLGSM:	Media layer gray scale median.
NS:	Non-significant differences.
SD:	Significant differences.
STD:	Standard deviation.
SS-TEL:	SS-Texture energy from SS-kernel.
$\phi_n(x,y)$:	n_{th}Instantaneous phase (IP) function.

I. Introduction

THE World Health Organization ranks cardiovascular disease (CVD: coronary artery disease, cerebrovascular disease, and peripheral artery disease) as the third leading cause of death and adult disability in the industrial world [1]. In the United Sates alone, 80 million American adults have one or more types of CVD, of whom about half are estimated to be age 65 or older. It is estimated that by 2015, there will be 20 million deaths due to atherosclerosis that will be associated with coronary heart disease and stroke.

Atherosclerosis causes enlargement of the arteries and thickening of the artery walls. It begins early in life and silently progresses until clinical events appear. Clinically, the IMT is used as a validated measure for the assessment of atherosclerosis [2] (see Fig. 1). It was proposed that not only the IMT, but also the ML, its thickness [3]–[6], and its textural characteristics [6]–[9] may be associated with the risk of developing stroke. Chambless *et al*. [10] showed that the IMT is a quantitative indicator of the extent of atherosclerosis, and therefore, IMT could be positively associated with an incident of stroke.

We illustrate the IMC, ML, and the IL in Fig. 1(a). As shown in Fig. 1, the IL is a thin layer, the thickness of which increases with age, from a single cell layer at birth to 250 μm at the age of 40 for nondiseased individuals [11]. In ultrasound images, the ML is characterized by a hypoechoic region, predominantly composed of smooth muscle cells, enclosed by the intima and adventitia layers (see Fig. 1, band Z6) [2], [6]. Earlier research [3] showed that the MLT does not change significantly with age (125 μm $<$ MLT $<$ 350 μm). In a study by Loizou *et al.* in 2009, the IMT, MLT, and ILT were estimated from 100 ultrasound images from 42 female and 58 male asymptomatic subjects. There were subjects of ages between 26 and 95 years old, with a mean age of 54 years. We measured the thickness to be: 1) IMT median of 0.66 mm with an IQR of 0.18 mm; 2) MLT median 0.23 mm with IQR of 0.18 mm; and 3) ILT median of 0.43 mm with IQR of 0.12 mm [5].

Loizou *et al*. in 2009 [9], found that: 1) there are significant differences between some texture features extracted from the IL, ML, and IMC (mean, GSM, STD, contrast, DV, periodicity); 2) some of the texture features can be associated with the increase (difference variance, entropy) or decrease (GSM) of patient's age; 3) the GSM of the ML falls linearly with increasing MLT and with increasing age; 4) the GSM of male subjects is larger than that of female subjects; and 5) male and female subjects may be better distinguished using texture features extracted from the IMC.

Our objective is to investigate the progression of textural characteristics of the IMC, ML, and IL of the CCA, through the use of new multiscale AM–FM methods [12]–[17] and combine them with standard texture features.

An input image $f(x,y)$ is expressed as the sum of its AM–FM components given by [15]

$$f(x,y) = \sum_{n=1}^{N} a_n(x,y)\cos\phi_n(x,y) \tag{1}$$

where $a_n(x,y)$ denote slowly varying IA functions, $\phi_n(x,y)$ denote the instantaneous phase (IP) components, and $n = 1,2,\ldots,N$ indexes the different AM–FM components. The AM–FM decomposition of (1) can be viewed as a generalization of the Fourier series decomposition in that it allows both the amplitude and phase functions to spatially vary. In particular, for each AM–FM component $a_n(x,y)\cos\phi_n(x,y)$, we define the instantaneous $\nabla\phi_n(x,y)$, and the magnitude of the IF, given by $\|\nabla\phi_n(x,y)\|$. For texture analysis, we are interested in using both the IA and the IF from different frequency scales. Here, we use the term frequency scales to refer to different ranges of the IF magnitude.

AM–FM models have been used in a variety of applications including image reconstruction [12], image retrieval [18], and video processing, such as motion estimation and video analysis [19]. A theoretical framework for understanding the role of multidimensional frequency modulation was reported in [20]. In [13], AM–FM texture features were compared to the classical texture features for the classification of carotid plaque ultrasound images. The study involved the use of 274 images (see also [21], 137 asymptomatic and 137 symptomatic). In this study, the AM–FM features performed slightly better than the classical texture features. A combination of the three-scale AM–FM representations produced the best results, reaching a classification success rate of 71.5%.

The basic multiscale AM–FM decomposition consists of estimating the IA, the IP, and the instantaneous frequency (IF) over

different scales. The term "instantaneous" refers to the fact that all AM–FM features vary as a function of pixel location. The promise of AM–FM methods can be summarized in that [17]: 1) they provide physically meaningful texture features [(e.g., IF in cycles per millimeter (mm)], over multiple scales, at pixel level resolution; 2) textures can be reconstructed from AM–FM components; 3) we can extract AM–FM decompositions for different frequency coverage; and 4) we have the recent development of robust methods for AM–FM demodulation (see examples in [15], [22]). We will elaborate on the AM–FM advantages in Section II.

In [4], a method was presented for quantifying the reflectivity of the ML of the distal CCA. The GSM of the IM layer gave the earliest change representing atherosclerotic disease in the arterial wall that can currently be imaged *in vivo*. In [23], the authors investigated the early structural changes of the CCA in familial hypercholesterolemia. Textural characteristics extracted from the IMC were found to be significantly different between patients with and without hypercholesterolemia. In [8], the authors reported on the properties of the GSM of the IMC from a random sample of 1016 subjects aged exactly 70. They found that the GSM of the IMC of the CCA is closely related to the echogenecity in overt carotid plaques.

While there are several studies reported earlier suggesting that the instability of the carotid atheromatous plaque can be characterized from B-mode ultrasound images [6], [21], we have not found any other studies reported in the literature, where the AM–FM characteristics (or any other multiscale features) of the IMC, ML, and IL have been shown to be associated with the risk of stroke. In [6] and [21], the echogenecity in atherosclerotic carotid plaques was evaluated through the GSM, where as in [9], the IMC, ML, and IL were characterized based on texture feature analysis. Visual inspections of the IMC in the CCA reveal that a great variation in echogenecity does exist. However, the usefulness of this information has not yet been studied.

II. Materials And Methods

A. Ultrasound Images Acquisition

A total of 100 B-mode longitudinal ultrasound images of the CCA were recorded using the ATL HDI-3000 ultrasound scanner (Advanced Technology Laboratories, Seattle, USA). The images were recorded at the Cyprus Institute of Neurology and Genetics in Nicosia, Cyprus. The recordings were carried out in agreement with the Cyprus national bioethics committee rules on clinical trials, and after patient's written consent. For the recordings, we used a linear probe (L74) with a recording frequency of 7 MHz [24]. Images were acquired with the subject's head rotated by 45° away from the study side. A single longitudinal image was captured at the distal end of the CCA, during the diastolic phase of a cardiac cycle. All captured images were revealing optimal visualization of the IMC of the far wall and the near wall of the CCA at the same time, thus, corresponding to a midline horizontal longitudinal representation of the CCA walls.

During image acquisition, the sonographers varied spatial resolution to provide optimal imaging at different depths [5], [9]. However, without standardizing image resolution, the estimated AM–FM components would not be comparable. To see this, note that continuous-space image frequencies are expressed in cycles per milimeter, and unless we have a common spatial resolution, the estimated digital frequencies would correspond to different continuous-space (analog) frequencies. As a result, we then had to use bicubic spline interpolation to resize all digital images to a standard pixel density of 16.66 pixels/mm. Here, we note that most images were acquired near this target resolution. In other words, we made small corrections to spatial resolution.

The images were also intensity normalized, as described in [25] and [26], where a manual selection of blood and adventitia performed by the user of the system is required. The gray-scale-intensity normalized image was obtained through algebraic (linear) scaling of the image by linearly adjusting the image so that the median-gray-level value of the blood was 0–5, and the median gray level of the adventitia (artery wall) was 180–190 [26], [27].

The images were recorded from 42 female and 58 male asymptomatic patients. These subjects had not developed any clinical symptoms, such as a stroke or a transient ischemic attack. The primary-care physicians informed the subjects of our stroke-prevention research study.

Overall, patient's ages varied between 26 and 95 years, with a mean age of 54 years. The images were partitioned into three different age groups. In the first group, we included 27 images from patients, who were younger than 50 years old. In the second group, we had 36 patients, who were 50–60 years old. In the third group, we included 37 patients who were older than 60 years.

Clinically, no significant changes are anticipated in the IMT before the age of 50 [28], [29]. Stroke incidences in this age group are more frequently associated with other causes than the usual cardiovascular risk factors (hypertension, hypercholesterolemia, smoking, etc.), like cardiac source of emboli, genetic factors, and others. Between the ages of 50 and 60, the age borderline for the young ($<$50 years) and the adult ($>$60 years) ages, a subtle increase in IMT can be demonstrated and IMC textural changes can be initially observed. Above the age of 60, IMT increases and changes in the IMC are more evident. Moreover, most of the stroke incidences in this age group are associated with the carotid atherosclerosis disease.

B. Manual Measurements

A neurovascular expert (neurologist) manually segmented (using the mouse) the IMC [25] the ML, and IL [5] on each image after image intensity normalization by selecting 20–40 consecutive points for the adventitia, media, and intima at the far wall. The measurements were performed between 1–2 cm proximal to the bifurcation of the CCA, on the far wall [2], over a distance of 1.5 cm. The bifurcation of the CCA was used as a guide and all measurements were made with reference to that region. The IMT, MLT, and the ILT were then calculated as the average of all vertical measurements taken at the interpolated

perpendicular distances between these structures. The measuring points and delineations were saved for further comparison. One of the authors (M. Pantziaris) performed the manual segmentation measurements (see also [5]).

C. IMC, ML, and IL Snake Segmentations

The IMC, ML, and IL regions were semiautomatically segmented from the images. The segmentation system is based on the Williams and Shah method [30], as documented in [5]. We first estimate an initial contour for the intima (I5) and adventitia (I7) using an initial contour estimation procedure proposed in [25]. We then segment the IMC using a semiautomated snakes-segmentation system [25], by deforming the initial estimated intima and adventitia boundaries, and extracting the final I5 (lumen–intima interface) and I7 boundaries (media–adventitia interface). The upper side of the ML (see Fig. 1, Z6) was then estimated by deforming the lumen–intima interface (boundary I5) by 0.36 mm (6 pixels) downward, and then deformed by the snakes-segmentation algorithm proposed in [5] and [25], in order to fit the media boundary. This displacement of 0.36 mm is based on the observation that the manual mean IMT lies between 0.54 mm (minimum of IMT mean) and 0.88 mm (maximum of IMTmean) with a mean IMT of 0.71 mm [25]. By taking into consideration that the spatial resolution (distance between two pixels) is 0.06 mm, then the IMT is lying within the range of 0.54–0.88 mm ($9 < \text{IMT} < 15$ pixels), with a mean of 0.71 mm (12 pixels). Thus, in order to estimate the MT, the displacement of the contour should be on average 0.36 mm (6 pixels times 0.06 mm) downward, which is half of the size of the IMT (the distance between I5 and I7, where I7 is the media–adventitia interface). In order to achieve standardization in extracting the thickness and AM–FM measures from the IMC, ML, and IL, segments with similar dimensions were divided based on the following procedure. A region of interest of 9.6 mm (160 pixels) in length was first extracted. This was done by estimating the center of the IMC area and then selecting 4.8 mm (80 pixels) left and 4.8 mm (80 pixels) right of the center of the segmented IMC. Selection of the same IMC, ML, and IL areas in length from each image is important in order to be able to extract comparable measurements between images and subject groups.

We note that there was no significant difference between the manual and automated segmentation measurements for the IMC, ML, and IL [5].

In the present study, in less than 8% of the cases, the positioning of the initial snake contour was not correctly calculated. There were another 6% of the cases, where the ML structure was very small and the two snake contours were trapped together. For these cases, the user of the proposed system may run the snakes initialization procedure again in order to estimate the correct initial snake contour, and during the snakes deformation the user may interact and manually correct the contour [5], [25].

D. AM–FM Methods

The basic AM–FM demodulation system is presented in Fig. 2(a). Here, the input image is first normalized. The normalized image is then processed using a Hilbert operator and a multiscale filterbank to produce AM–FM features associated with each channel filter. The dominant features over the low-, medium-, and high-frequency scales are then selected as the outputs of the method. In what follows, we provide a step-by-step summary of the employed AM–FM method. We refer to [16] for full details on the method. First, we normalize each input image to a maximum image intensity of 1. Please recall that the spatial resolution was also standardized prior to any further processing. Then, for the segmented IMC, ML, and IL images, we first computed an extended version of the 1-D analytic signal, as given in [16]

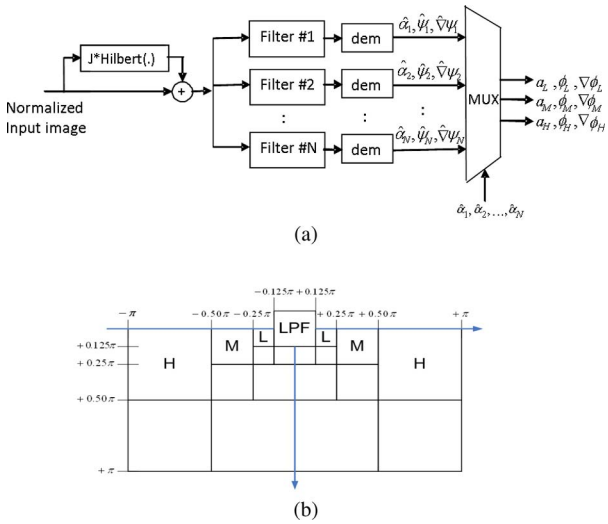

Fig. 2. AM–FM demodulation system: (a) system diagram; (b) effective spectral coverage of dyadic filterbank with low, medium, and high bandpass-channel filters centered around the horizontal frequencies. The effective spectral coverage is achieved using an extended Hilbert transform operator, followed by a 2-D, separable filterbank [16]. Due to the inherent symmetry of frequency components for real-images, expressed as $F(u,v) = F^*(-u,-v)$ in the spectral domain, we note that the upper two-quadrants can be inferred from the lower ones (see [16] for details on the method). Also, the maximum image intensity in the input image is normalized to 1.0.

$$\widehat{f}_{\,\mathrm{AS}}(x,y) = f(x,y) + jH_{2-\mathrm{D}}[f(x,y)] \tag{2}$$

where $f(x,y)$ denotes the input image, and $H_{2-\mathrm{D}}$ denotes the 2-D Hilbert transform operator applied along the columns. The next step requires the application of a 2-D filterbank that covers the discrete frequency space (see Fig. 2(b)).

In what follows, we will describe the method for generating AM–FM component estimates over each 2-D channel filter. A basic requirement is that each IF estimate falls within the pass-band of the filter [16]. For the current application, we note that we have horizontal image structures, which are thin in the vertical direction. The thin spatial spread in the vertical direction results in a wide vertical frequency spread. In other words, we have strong vertical edge artifacts that do not necessarily represent texture. To avoid these artifacts, we do not generate AM–FM components from the LPF and channel filters with large vertical components. Thus, we only consider AM–FM estimates from filters adjacent to the horizontal frequency axis. Based on the magnitude of the estimated IF, we

label the remaining filters as "L" for low, "M" for medium, and "H" for high frequency (see Fig. 2(b)). To further reduce edge artifacts, we consider only AM–FM measurements that are within the segmented regions of each structure.

We use the outputs of each bandpass filter to estimate the IA, IP, and IF. This demodulation step is labeled as "dem" in Fig. 2(a). The IA is given by the absolute value of the complex-valued output. The IP is given as the angle of the channel filter output. The estimation of the IF requires a small number of additional steps.

First, we normalize the output from each filter using [12], [16]

$$\bar{f}_{\mathrm{AS},i}(x,y) = \widehat{f}_{\mathrm{AS},i}(x,y)/|\widehat{f}_{\mathrm{AS},i}(x,y)| \tag{3}$$

where $\widehat{f}_{\mathrm{AS},i}(x,y)$ denotes the output of the ith filter. Second, we consider IF estimates based on

$$\frac{d\varphi(x,y)}{dx} \cong \frac{1}{n}\arccos\left(\frac{\bar{f}_{\mathrm{AS},i}(x+n,y)+\bar{f}_{\mathrm{AS},i}(x-n,y)}{2\bar{f}_{\mathrm{AS},i}(x,y)}\right) \tag{4}$$

and similarly for $d\varphi/dy$. In (4), we consider $n = 1, 2, 3, 4$ for the low frequencies, $n = 1, 2$ for the medium frequencies, and $n = 1$ for the high frequencies. Among the IF estimates, we select the one that generates the minimum argument to the $\arccos(.)$ function. This also happens to give the minimum condition number for the function evaluation. Similarly, we estimate the IF component along the y-direction. As mentioned earlier, if the estimated IF falls outside the support of the bandpass filter, then it is considered as inaccurate.

At each pixel, for each scale (low/medium/high passbands), we select between two possible AM–FM component estimates. This is done by selecting the AM–FM features that give the largest IA estimate. The procedure is known as DCA, which is illustrated using the MUX block in the system diagram of Fig. 2(a).

For the IA features, we will use the terms low-IA, medium-IA, and high-IA to refer to IA estimates derived from the different channels. For the IF, we will use the terms low-IF, medium-IF, and high-IF to refer to the derived IF magnitude estimates. We normalize the IF magnitude estimates to cycles/mm, providing a physically meaningful interpretation of the texture measurements. Furthermore, please note that the normalization of the maximum-input image intensity corresponds to the normalization of the IA estimates.

E. Statistical Analysis

The Mann–Whitney rank sum test (for independent samples of different sizes) is used in order to identify if there are SD or NS between the extracted AM–FM features. For significant differences, we require $p < 0.05$ and compare between age groups and between male and female subjects. We use median values over the segmented components to investigate the relationships between the three different age groups for the IMC, ML, and IL. Similarly, for comparing independent samples from equal populations, we use the Wilcoxon rank sum test to detect texture and AM–FM feature differences between the IL, ML, and IMC, for both manual and automated segmentations. We also use box plots to compare between IMC, ML, and IL, and between HIA, MIA, and LIA amplitude.

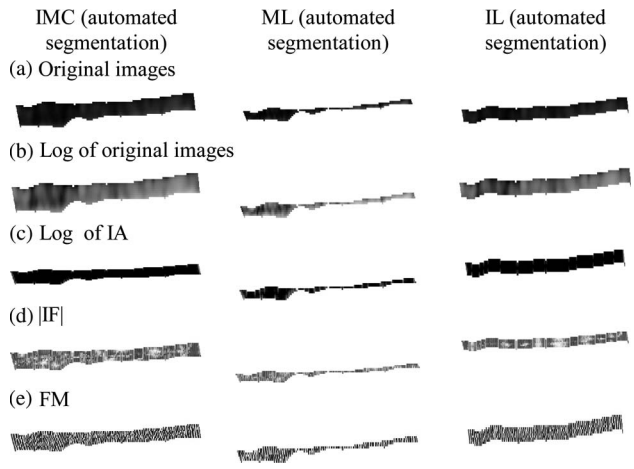

Fig. 3. High-scale AM–FM analysis of the IMC, ML, and IL for a male asymptomatic subject aged 54. (a) Original IMC (left column), ML (middle column), IL (right column) images; (b) logarithm view of IMC, ML, and IL; (c) logarithm view of the medium-scale IA; (d) |IF| of IMC, ML, and IL; (e) medium-scale FM reconstruction of IMC, ML, and IL. Note that IF estimates with magnitudes outside the support of the medium-scale passbands are not shown.

III. Results

We present several results to show that AM–FM texture features can be used to differentiate between the different age groups. We also investigate AM–FM texture feature sensitivity to sex and compare with classical texture features from [9].

We provide an example for AM–FM texture analysis in Figs. 3 and 4. In Fig. 3, the IMC (see Fig. 3(a) left column), ML (see Fig. 3(a) middle column), and the IL (see Fig. 3(a) right column) were extracted using automated segmentations, as described in [5]. For this example, we have IMT = 0.79 mm, MLT = 0.32 mm, and ILT = 0.47 mm. For better visualization, the digital images of the IMC, ML, and IL have been interpolated to be 300×20 pixels. Fig. 3(a) through Fig. 3(e) present high-scale AM–FM estimates for comparing the IMC (left column), ML (middle column), and IL (right column) from a male asymptomatic subject aged 54. We show the original images of the IMC, ML, and IL in the first row of Fig. 3(a). For better visualization of these images, we also present the logarithmic versions of these figures in Fig. 3(b). These images were generated by simply taking the log(.) of the images in Fig. 3(a). Similarly, we present the logarithmic version of the IA in Fig. 3(c). The IF magnitude IF is shown in Fig. 3(d), and the FM images in Fig. 3(e). The FM images refer to $\cos(\phi)$ (see (1)).

Fig. 4 presents a comparison of the cumulative density functions from the images in Fig. 3 in terms of the intensity and IA (see Fig. 4(a)), IF in both the horizontal and vertical directions (see Fig. 4(b)) and comparison in terms of the IF magnitude IF (see Fig. 4(c)).

Table I presents a comparison of the mean, STD, median, 25%, 75% quartiles, and IQR between the high, medium, and low AM–FM features extracted from the IMC, ML, and IL for

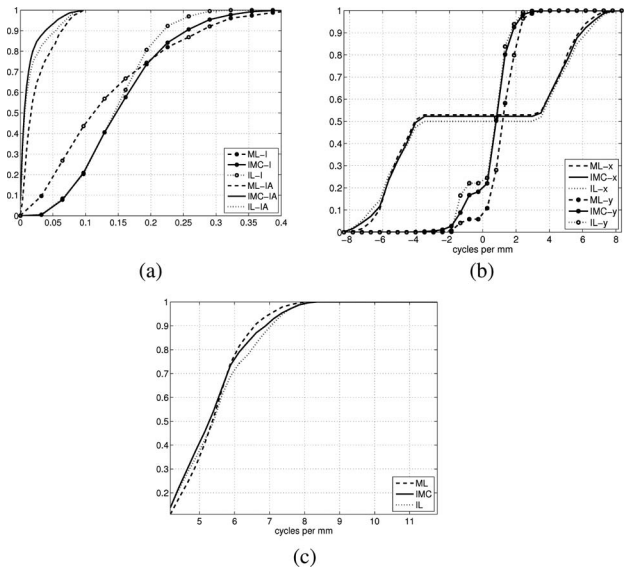

Fig. 4. High-scale AM–FM analysis example. This figure provides a comparison of the cumulative density functions (CDfs) from the images in Fig. 3. Results for the IMC are presented using solid lines, for ML we use ''–'' lines and IL with dotted (''. . .'') lines. (a) Comparison in terms of image intensity (I) and IA; (b) comparison in terms of IF in the x and y directions; and (c) comparison in terms of |IF| magnitude.

the automated segmentation measurements for the three different age groups, below 50 (<50), between 50 and 60 (50–60), and above 60 (>60) years old. The results indicate that for the HIF magnitude median for the ML, the 75th percentile value of the >60 age group remains lower than the median value of the 50–60 age group (5.59 < 5.61 cycles/mm). For the IL, we similarly observe that the 75th percentile of the low-scale median IA for the >60 group remains significantly lower than the median of the 50–60 group (4.10 < 4.28 hundreds, see last two rows in Table I).

We provide a list of AM–FM and classical texture features that showed significant differences among age groups and anatomical structures in Table II (classical texture features results taken from [9]). AM–FM features can be used to differentiate among several different age groups from each structure (IMC, ML, IL). Based on the dyadic frequency decomposition, we have 1) low-frequency components from 1.04 to 2.95 cycles/mm that correspond to IWs from 5.66 to 16 pixels (0.34–0.96 mm); 2) medium-frequency components from 2.08 to 5.89 cycles/mm that correspond to IW from 2.83 to 8 pixels (0.17–0.48 mm); and 3) high-frequency components from 4.17 to 11.79 cycles/mm that correspond to IW from 1.41 to 4 pixels (0.085–0.24 mm).

For the AM–FM features that could be used to detect significant textural differences between age groups, we present box plots in Fig. 5. We present box plots for the IA from the low- and medium-frequency scales, and IF magnitude from high-frequency scales. We summarize results from all age groups and both sexes in the left column. We present separate results from the two sexes (all age groups) in the right-column plots.

In Table III, we compare AM–FM feature differences associated with differences in sex. Here, we note that the IA for the ML showed significant differences between males and females

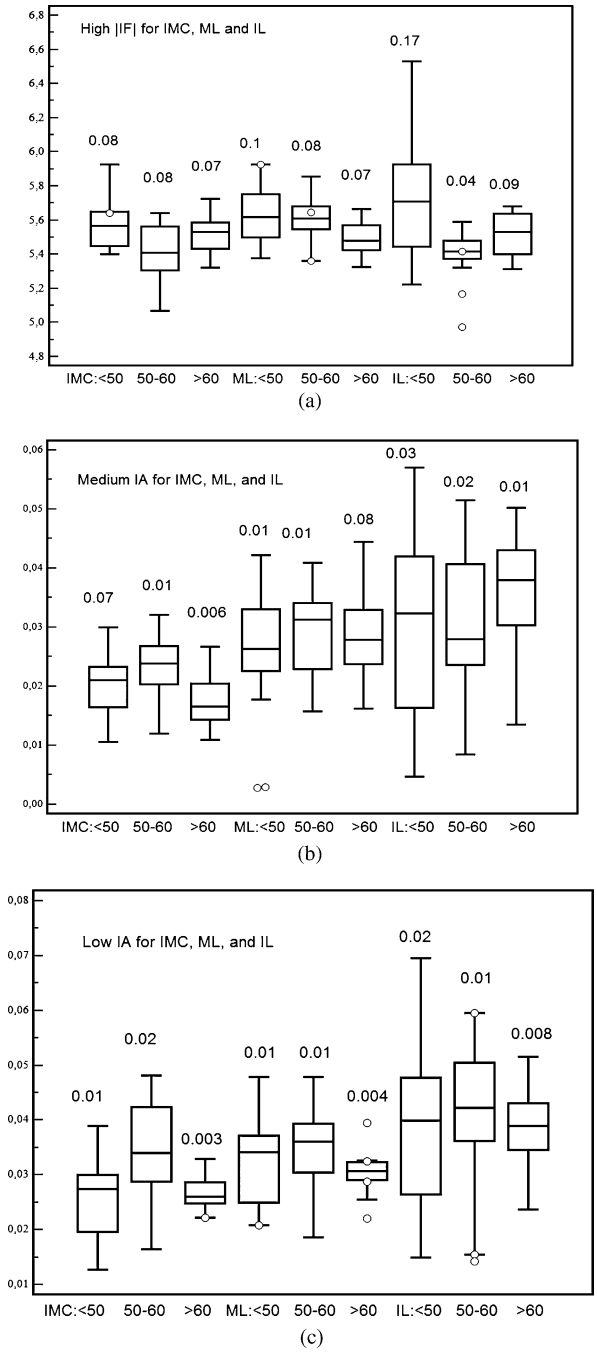

Fig. 5. Box plots for the IA and IF magnitude for IMC, ML, and IL for different scales, age groups. (a) High-frequency scale IF magnitude. (b) Medium-frequency scale results. (c) Low-frequency scale IA results. For each we also present the age group and anatomical location. IQR values are shown above the box plots. In each plot we display the median, lower, and upper quartiles and confidence interval around the median. Straight lines connect the nearest observations with 1.5 of the Inter-quartile range (IQR) of the lower and upper quartiles. Unfilled circles indicate possible outliers with values beyond the ends of the 1.5 × IQR. Here, we note that the input image has been normalized, where the maximum image intensity value is 1.0.

for all age groups. We refer to the plots of Fig. 5 for the IA differences between males and females. It is also interesting

TABLE I
COMPARISON OF THE MEAN, STANDARD DEVIATION (STD), MEDIAN, LOWER QUARTILE (P25%), UPPER QUARTILE (P75%), AND INTER-QUARTILE RANGE (IQR) BETWEEN THE HIGH, MEDIUM, AND LOW AM–FM FEATURES EXTRACTED FROM THE IMC, ML, AND IL FOR THE AUTOMATED SEGMENTATION MEASUREMENTS FOR THE THREE DIFFERENT AGE GROUPS, BELOW 50 (<50), BETWEEN 50 AND 60 (50–60), AND ABOVE 60 (>60) YEARS OLD. HERE, THE IA VALUES HAVE BEEN PREMULTIPLIED BY 100 FOR BETTER VISUALIZATION. RECALL THAT THE ORIGINAL IMAGES WERE NORMALIZED TO A MAXIMUM BRIGHTNESS VALUE OF 1. THUS, THE IA VALUES REPRESENT A PERCENTAGE OF THE MAXIMUM INPUT IMAGE INTENSITY. THE INSTANTANEOUS FREQUENCY MAGNITUDE, IF, IS MEASURED IN CYCLES/MM

		Mean	STD	Median	P25%	P75%	IQR
IMC	MIA:<50	2.01	0.50	2.00	1.62	2.33	0.70
	MIA:>60	1.82	0.44	1.82	1.48	2.1	0.62
	LIA:<50	2.62	0.80	2.55	1.89	3.00	1.11
	LIA: >60	2.71	0.35	2.68	2.50	2.89	0.39
	HIF:50-60	5.46	0.18	5.43	5.33	5.56	0.22
	HIF: >60	5.51	0.12	5.50	5.40	5.59	0.20
ML	LIA: <50	3.34	0.90	3.42	2.50	3.70	1.20
	LIA:50-60	3.70	0.87	3.60	3.04	4.27	1.23
	HIF:50-60	5.62	0.18	5.61	5.54	5.74	0.20
	HIF: >60	5.52	0.14	5.51	5.42	5.59	0.17
IL	LIA:50-60	4.26	1.31	4.28	3.59	4.93	1.34
	LIA: >60	3.67	1.90	3.81	3.30	4.10	0.80

IMC: Intima-media complex, ML: Media layer, IL: Intima layer.

TABLE IA
AUTOMATED IMC, ML, AND IL SEGMENTATIONS IN MILLIMETERS FOR THE THREE DIFFERENT AGE GROUPS, BELOW 50 (<50), BETWEEN 50 AND 60 (50–60), AND ABOVE 60 (>60) YEARS OLD. HERE, THE IA VALUES HAVE BEEN PREMULTIPLIED BY 100 FOR BETTER VISUALIZATION

		Mean	STD	Median	P25%	P75%	IQR
IMT	IMT: All	0.67	0.12	0.66	0.58	0.76	0.12
	IMT: <50	0.61	0.11	0.59	0.54	0.64	0.09
	IMT:50-60	0.68	0.10	0.69	0.61	0.73	0.12
	IMT: >60	0.74	0.13	0.73	0.69	0.80	0.11
MLT	ML: All	0.25	0.11	0.25	0.16	0.34	0.18
	ML: <50	0.19	0.11	0.17	0.13	0.23	0.09
	ML:50-60	0.26	0.10	0.26	0.19	0.32	0.12
	ML: >60	0.32	0.13	0.11	0.29	0.38	0.11
ILT	IL: All	0.42	0.01	0.42	0.41	0.42	0.01
	IL: <50	0.42	0.01	0.42	0.41	0.42	0.01
	IL: 50-60	0.42	0.01	0.42	0.40	0.41	0.01
	IL: >60	0.42	0.01	0.42	0.42	0.42	0.01

IMT: Intima-media thickness, MLT: Media layer thickness, ILT: Intima layer thickness.

TABLE II
COMPARISON BETWEEN THE HIGH, MEDIUM, AND LOW AM–FM AND CLASSICAL TEXTURE FEATURES EXTRACTED FROM THE IMC, ML, AND IL FOR THE AUTOMATED SEGMENTATION MEASUREMENTS FOR THE THREE DIFFERENT AGE GROUPS, BELOW 50 (<50), BETWEEN 50 AND 60 (50–60), AND ABOVE 60 (>60) YEARS OLD (FIRST THREE COLUMNS) BASED ON THE MANN–WHITNEY RANK SUM TEST. ONLY THE FEATURES THAT EXHIBITED SIGNIFICANT DIFFERENCES AT $p < 0.05$ ARE SHOWN

		Instantaneous Amplitude (IA) and Instantaneous Frequency (IF) magnitude					
		IMC		ML		IL	
		50-60	>60	50-60	>60	50-60	>60
AM-FM Texture Features Low-Medium-High	<50	Low-scale IA, Medium-scale IA High-scale |IF|		Low-scale IA			
	50-60			High-scale |IF|		Low-scale IA	
Classical Texture Features [9]	<50	GSM, STD, DV, Entropy		GSM, SS-TEL	GSM, STD Contrast, DV, Complexity, Coarseness, SS-TEL		Complexity

IMC: Intima-media complex; ML: Media layer; IL: Intima layer; GSM: Gray scale median; STD: Standard deviation; DV: Difference variance; SS-TEL: SS-Texture energy from SS Kernel.

TABLE III
COMPARISON BETWEEN SEX GROUPS (MALE/FEMALE) FOR THE IMC, ML, AND IL AM-FM HIGH, MEDIUM, AND LOW FREQUENCIES FEATURES FOR THE INSTANTANEOUS AMPLITUDE (IA) AND THE INSTANTANEOUS FREQUENCY (IF) USING THE MANN WHITNEY RANK SUM TEST

	IMC		ML		IL	
Male/Female	IA	IF	IA	IF	IA	IF
High Freq.	NS (0.25)	NS (0.16)	S (0.002)	NS (0.72)	NS (0.24)	NS (0.16)
Medium Freq.	S (0.04)	NS (0.67)	S (0.0007)	NS (0.46)	S (0.03)	NS (0.57)
Low Freq.	NS (0.09)	NS (0.93)	S (0.002)	NS (0.09)	NS (0.18)	NS (0.97)

IMC: Intima-media complex; ML: Media layer; IL: Intima layer. The p value is also shown in parentheses. (S = Significant difference at $p < 0.05$).

to note that the IF magnitude from high scales did not show significant differences related to sex. The IF distributions for high scales appear to be very similar (see Fig. 5(b)).

We now want to examine significant trends through the ages using box plots and regression analysis. From Fig. 5 and Tables I–III, for the age groups from 50–60 to >60, we can see several significant changes. We focus on the ML and IL: 1) for the ML, the high-scale IF magnitude median (±IQR) undergoes a significant drop from 5.61 (±0.20) cycles/mm for the 50–60 age group to 5.51 (±0.17) cycles/mm for the >60 group ($p = 0.004$). We also see a significant increase in the low-scale IA median (±IQR) value from 3.42 (±1.20) hundreds for the <50 age group to 3.60 (±1.23) hundreds for the 50–60 group ($p = 0.0033$). Furthermore, we did not find that these changes depended on sex; 2) for the IL, the low-scale IA median (±IQR) value shows a drop from 4.28 (±1.34) hundreds from 50–60 to 3.81 (±0.80) hundreds for the >60 age group ($p = 0.026$).

From these findings, it is clear that we have different textural changes occurring in the ML and the IL.

In summary from Table II, we observe the following.

1) Significant differences in IMC texture between the age group of over 60 and younger. a) For the <50 and >60

years old using the texture features GSM, STD, DV, and entropy, or medium-scale IA. b) For ages 50–60 and >60 years old using the texture features STD and contrast or using low-scale IA or high-scale |IF| magnitude.

2) Significant differences in ML texture between any two age groups: a) For ages <50 and 50–60 years old using the texture features GSM, and SS-TEL, or low-scale IA. b) For ages <50 and >60 years old using the texture features GSM, STD, contrast, DV, complexity, coarseness, and SS-TEL. c) For ages 50–60 and >60 years old using the texture feature coarseness or using high-scale |IF|.
3) Significant differences in IL texture between the age group of over 60 and younger: a) For the ages <50 and >60 years old using the texture feature complexity, or low-scale IA. b) For the ages 50–60 and >60 years old using low-scale IA.

Regression analysis demonstrated that there was no linear relation among the low-, medium-, and high-scale IA and IF components with age.

IV. Discussion

In this study, we investigated AM–FM features extracted from the IMC, ML, and IL of 100 ultrasound images of the CCA of asymptomatic subjects. In summary, we found significant texture differences between the higher risk age group of >60 years versus the lower risk age group of <50 and the 50–60 group. In particular, between the <50 and >60 groups, we found significant differences in the medium-scale IA extracted from the IMC. Between the >60 and the 50–60 groups, we found significant texture changes in the low-scale IA and high-scale IF magnitude extracted from the IMC, and the low-scale IA extracted from the IL. Also, we note that the IA for the ML showed significant differences between males and females for all age groups. The AM–FM features provide complimentary information to classical texture analysis features like the gray-scale median (GSM), contrast and coarseness.

From Table I, for the HIF magnitude median for the ML, we observe that the 75th percentile value of the >60 age group remains lower than the median value of the 50–60 age group (5.59 < 5.61 cycles/mm). The median value drop represents a reduction of about half a STD of the distribution of the median frequency of the 50–60 group. Furthermore, as demonstrated in the FM plots of Figs. 3 and 4, this reduction corresponds to the horizontal frequency components that span across the long side of the ML. Given the high-IF magnitude range of 4.17–11.79 cycles/mm, we can see that the median IF magnitude is concentrated on the lower half of the high-frequency spectrum (5.6 cycles/mm is closer to 4.17 than to 11.79 cycles/mm). A possible explanation of the significant drop may be due to the spatial growth of the high-frequency components. In other words, spatial growth of these high-frequency components may have led to a shrinkage in the frequency domain, as suggested by the uncertainty principle. Furthermore, we note that this spatial growth was not seen in the lower and middle frequency ranges.

For the IL, we similarly observe that the 75th percentile of the low-scale median IA for the >60 group remains significantly lower than the median of the 50–60 group (4.10 < 4.28 hundreds). Furthermore, the drop of the IA is about half an STD of the variation. Compared to the fine changes of the high-frequency components, recall that these lower frequency components range from 1.04 to 2.95 cycles/mm. The drop in the low-scale IA over these components suggests that any growth or change will have to be attributed to finer, higher frequency scales.

The AM–FM features that gave significant differences, as documented in Table II, are as follows: 1) the IMC age group of the >60 can be differentiated from the <50 group using the medium-scale IA, and from the 50–60 group using the low-scale IA, and/or high-scale IF; 2) the ML age group of 50–60 can be differentiated from the <50 group using the low-scale IA, and from >60 group using the high-scale IF; and 3) the IL age group of >60 can be differentiated from the 50–60 group using the low-scale IA.

We have found in [9], a decrease of the GSM of the ML (MLGSM) with increasing age (59.7 $\pm$ 12.9, 49.9 $\pm$ 22.0, 33.6 $\pm$ 25.8 for the age groups <50, 50—60, and >60, respectively), as well as decrease with thickness (MLT). The decrease in the MLGSM suggests an increase in the hypoechoic (echolucent) structures. This may be due to an increased concentration of lipids (which appear hypoechoic) and hyperplasia of muscle fibers in the ML in early atherosclerosis [31]. The MLGSM of male patients (47.9 $\pm$ 20.7) was shown to be brighter than that of the female (40.5 $\pm$ 17.5) patients. The GSM of the IMC (IMCGSM) for the age groups <50, 50–60, and >60 was 39.2 $\pm$ 13.6, 25.8 $\pm$ 18.1, and 27.6 $\pm$ 14.4), while the ILGSM (the GSM of the intima layer) was 38.6 $\pm$ 17.2, 39.4 $\pm$ 15.8, and 32.8 $\pm$ 15.7, respectively. The GSM values for the IMC, ML, and IL for all patients were 30 $\pm$ 21.3, 28 $\pm$ 18, and 35$\pm$18.5, respectively. Furthermore, some other classical texture features used in [9] gave significant differences between age groups. More specifically, for ages <50 and >60, the texture features STD ($p = 0.03$, $p = 0.04$, $p = 0.01$ for IMC, ML, and IL, respectively), contrast ($p = 0.001$ for IL), complexity ($p = 0.0001$ for IL), and coarseness ($p = 0.004$ for the ML) showed significant differences. The SS-texture energy from SS-kernel (Laws texture energy measures) gave significant different values for the ML for <50 and 50–60 ($p = 0.04$) and the entropy for the IMC for <50 and >60 ($p = 0.04$).

In [8], the authors reported on the properties of the GSM of the IMC from a random sample of 1016 subjects aged exactly 70. More specifically, for the CCA, they showed that the GSM of the IMC was correlated to GSM in the plaque independently of plaque size and IMT. This finding suggests that the GSM and maybe other texture features extracted from the ML can be important and easily measurable characteristics of the CCA wall that may have prognostic impact for assessing CVD risk.

Previously, GSM analysis has been performed mainly on plaques. The GSM was found to be related to histological features of the plaque, such as the elastin and calcium content, as well as to the size of the lipid-rich necrotic core [32]. From [4], the GSM of the IMC may be the first marker of atherosclerosis and may precede the development of significant increase in IMT. This would enable earlier identification of high-risk

individuals based on the analysis of the CCA artery-wall textural characteristics. In [33], the authors observed an increase in the granularity in association with atherosclerotic disease, where a granular IMC indicated more advanced atherosclerosis.

In what follows, we will attempt to relate the significant differences in AM–FM features to structural differences. In essence, the multiscale AM–FM analysis allows us to associate structural changes to different structures (IMC, ML, and IL). As noted earlier, we have a drop in the low-scale IA of the IL with increasing age (see Fig. [5](e)). Since the image brightness is normalized to a maximum of 1, the reduction in the median low-scale IA may be attributed to the appearance of new, brighter-appearing (echogenic) structures. Here, we are making the association between brighter regions and high values of the IA (see (1)). Clinically, this may be due to the deposition/accumulation of calcium (echogenic) within the arterial walls, a process not completely understood, that can occur early in the process of atherosclerosis [34]. The association between echogenic pixels and calcium is based on histology [32]. However, echogenic pixels may also be due to elastin [32]. Thus, our association of bright components with calcium changes has to be further investigated.

This implies structural instability of the IL with increasing age. Here, it is interesting to note that the GSM describes variations over all scales, while our multiscale IA analysis enables us to associate these changes with different structural component sizes.

The reduction in the ML high-scale IF magnitude may be associated with thickening of the fine structures (see Fig. 5(a)). Here, we are making the association between high frequencies and fine structures. An enlargement of finer structures will lower the IF magnitude. However, further studies are needed to establish the associations between finer structures and actual plaque components (such as calcium, lipid cores, etc). Overall, as seen in Fig. 5, we have nonlinear trends in most AM–FM features. Our focus has been to provide an interpretation for significant differences of the ML and IL between the 50–60 with the >60 groups.

The intensity normalization method used in this study was found to be helpful in the manual contour extraction [27], as well as the snakes segmentation of the IMC [25] and the atherosclerotic carotid plaque segmentation [35]. Moreover, this method increased the classification accuracy of different plaque types as assessed by the experts [36]. Ultrasound image normalization was carried out prior to the segmentation of the IMT on carotid artery ultrasound images for increasing the image contrast in [37].

Our clinical interests are in the development of an early diagnosis and prevention system that can provide a measure of the risk levels prior to any symptoms. Clearly, it is difficult to assess stroke risk levels prior to any symptoms. Having said this, it is well established that the risk of stroke increases with age [31]. Thus, we are very interested in understanding how atherosclerotic texture changes as a function of age. To this end, we carefully selected normal subjects that have not developed any clinical symptoms of stroke or transient ischemic attack. Clinically, as a measure of risk increase, we have verified that this population exhibits a strong correlation and a linear increase in the size of the IMT as a function of age [5], [9].

Some limitations of the proposed method that were also documented in [5] are briefly presented. One of the limitations is the presence of strong speckle noise, which hinders the visual and automatic analysis in ultrasound images [27]. Such images were not included in this study. Backscattered ultrasound is also angle dependent. During image acquisition, a standard clinical protocol was followed, where the position of the probe was adjusted so that the ultrasound beam was at right angles to the arterial wall (see Section II and II-A). This improved the IMC visualization. Although, the ultrasound images used in this study showed a horizontal representation of the CCA, the snake-segmentation algorithm [25] used to segment the images was also tested in images with plaques and curved segments [35], and is now being tested in a larger multiinstitutional database of 400 images. Currently, this study is giving very satisfactory results, with only 4%–6% of the images being discarded. The new spatial compound imaging technique might optimize further carotid plaque imaging [26], [31]. Furthermore, only vessels without atherosclerotic plaques were segmented in this study because the proposed snakes-border-detection method does not apply to cases, where the IMT is larger than 1.4 mm. For larger IMT, a different initialization procedure based on plaque segmentation should be followed (see [35]).

Our AM–FM texture analysis is limited by the thin layers we are analyzing. The application of digital bandpass filters will result in boundary artifacts. We have managed to reduce these effects by reporting on the segmented regions and focusing on bandpass channel filters with substantial horizontal components. However, even the horizontal frequency components are affected by the left and right boundaries. As part of our long-term research plan, we are currently investigating algebraic methods that do not depend on convolution filtering.

Risk factors such as smoking, blood pressure, inflammation markers, life style, and cholesterol correlate to the traditional carotid IMT [1], [11], [23], [26], [31], [32], and are also important. It would be valuable to relate these risk factors to AM–FM characteristics extracted from the IL, ML, and IMC. Ongoing studies from our group will give more findings on this topic.

V. Concluding Remarks

The AM–FM analysis presented in this study showed that AM–FM features extracted from the IL, ML, and IMC may be used to distinguish between age groups and male and female patients. AM–FM analysis reveals that the IA for all scales and all structures (IMC, ML, and IL) decreases from the 50–60 to the >60 age group (see Fig. 5). This decrease in IA, similar to the reported decrease of the GSM of the ML of the CCA [9], may be attributed to the deposition/accumulation of calcium (echogenic) within the arterial walls that can occur early in the process of atherosclerosis [34]. This is a potential biomarker associated with increased risk of stroke with increasing age. Clinically, vascular wall calcification is a marker of atherosclerosis, which increases with age and thus increases the risk for cardiovascular events [38], [39].

The proposed methodology may also be applied to subjects who have already developed atherosclerotic plaques in order to study the contribution of the ML texture features to cardiovascular risk. For these subjects, we want to prognose future cardiovascular events.

REFERENCES

[1] American Heart Association, *Heart Disease And Stroke Statistics,* update, Dallas, Texas, 2007.

[2] P. Pignoli, E. Tremoli, A. Poli, P. Oreste, and R. Paoletti, "Intima plus media thickness of the arterial wall: A direct measurement with ultrasound imaging," *Atherosclerosis*, vol. 74, no. 6, pp. 1399–1406, 1986.

[3] E. J. Gussenhoven, P. A. Frietman, S. H., R. J. van Suylen, F. C. van Egmond, C. T. Lancee, H. van Urk, J.R. Roelandt, T. Stijnen, and N. Bom, "Assessment of medial thinning in atherosclerosis by intravascular ultrasound," *Am. J. Cardiol.*, vol. 68, no. 17, pp. 1625–1632, 1991.

[4] S.M. Ellis and P. S. Sidhu, "Granularity of the carotid artery intima-medial layer: Reproducibility of quantification by a computer based program," *British J. Radiol.*, vol. 73, no. 870, pp. 595–600, 2000.

[5] C.P. Loizou, C. S. Pattichis, A. N. Nicolaides, and M. Pantziaris, "Manual and automated media and intima thickness measurements of the common carotid artery," *IEEE. Trans. Ultr. Fer. Freq. Contr.*, vol. 56, no. 5, pp. 983–994, May 2009.

[6] M. L. Grønhold, B. G. Nordestgaard, T. V. Schroeder, S. Vorstrup, and H. Sillensen, "Ultrasonic echolucent carotid plaques predict future strokes," *Circulation*, vol. 104, no. 1, pp. 68–73, 2001.

[7] Q. Liang, I. Wendelhag, J. Wilkstrand, and T. Gustavsson, "A multiscale dynamic programming procedure for boundary detection in ultrasonic artery images," *IEEE Trans. Med. Imag.*, vol. 19, no. 2, pp. 127–142, 2000.

[8] L. Lind, J. Andersson, M. Roenn, and T. Gustavsson, "The echogenecity of the intima-media complex in the common carotid artery is closely related to the echogenecity in plaques," *Atherosclerosis*, vol. 195, no. 2, pp. 411–414, 2007.

[9] C.P. Loizou, M. Pantziaris, M. S. Pattichis, E. Kyriakou, and C. S. Pattichis, "Ultrasound image texture analysis of the intima and media layers of the common carotid artery and its correlation with age and gender," *Comp, Med. Imag. Graph.*, vol. 33, no. 4, pp. 317–324, 2009.

[10] L. E. Chambless, A. R. Folsom, L. X. Clegg, A. R. Sharrett, E. Shahar, F. J. Nieto, W. D. Rosamond, and G. Evans, "Carotid wall thickness is predictive of incident clinical stroke: The atherosclerosis risk in communities (ARIC) study," *Am. J. Epidemiol.*, vol. 151, no. 5, pp. 478–487, 2000.

[11] C. D. Mario, G. Gorge, R. Peters, F. Pinto, D. Hausmann, C. von Birgelen, A. Colombo, H. Murda, J. Roelandt, and R. Erbel, "Clinical application and image interpretation in coronary ultrasound: Study group of intracoronary imaging of the working group of coronary circulation and of the subgroup of intravascular ultrasound of the working group of echocardiography of the European Society of Cardiology," *Eur. Heart J.*, vol. 19, no. 2, pp. 201–229, 1998.

[12] V. Murray, P. Rodriguez, and M. S. Pattichis, "Robust multiscale AM-FM demodulation of digital images," *IEEE Int. Conf. Image Proc.*, vol. 1, pp. 465–468, Oct. 2007.

[13] C. I. Christodoulou, C. S. Pattichis, V. Murray, M. S. Pattichis, and A. N. Nicolaides, "AM-FM representations for the characterization of carotid plaque ultrasound images," in *Proc. 4th Eur. Conf. Int. Feder. Med. Biolog. Eng. (MBEC) '08*, Antwerp, Belgium, Nov. 23–28, 2008, pp. 1–4.

[14] J. P. Havlicek "AM-FM image models," Ph.D. dissertation, Dept. Electr. Comput. Eng., The University of New Mexico, Albuquerque, New Mexico, (1996). [Online]. Available: http://hotnsour.ou.edu/joebob/PdfPubs/JPHavlicekDiss.pdf

[15] V. M. Murray Herrera "AM-FM methods for image and video processing," Ph.D. dissertation, Dept. Electr. Comput. Eng., Univ. New Mexico, Albuquerque, New Mexico, Sep. 2008.

[16] V. Murray, P. Rodriquez, and M. S. Pattichis, "Multi-scale AM-FM demodulation and reconstruction methods with improved accuracy," *IEEE Trans. Imag. Proces.*, vol. 19, no. 5, pp. 1138–1152, May. 2010.

[17] M. S. Pattichis, "Multidimensional AM-FM models and methods for biomedical image computing," in *Proc. 34th IEEE Ann. Int. Conf. Eng. Med. Biol. Soc.*, Sep. 2–6, 2009, pp. 5641–5644.

[18] V. Murray, M. S. Pattichis, and P. Soliz, "New AM-FM analysis methods for retinal image characterization," in *Proc. 42nd IEEE Asilomar Conf. Signals, Syst. Comput.*, 2008, pp. 664–668.

[19] V. Murray, S. Murrilo, M. S. Pattichis, C.P. Loizou, C. S. Pattichis, E. Kyriakou, and A. Nicolaides, "An AM-FM model for motion estimation in atherosclerotic plaque videos," in *Proc. 41st IEEE Asilomar Conf. Signals, Syst. Comput.*, Nov. 4–7, 2007, pp. 746–750.

[20] M. S. Pattichis and A. C. Bovik, "Analyzing image structure by multidimensional frequency modulation," *IEEE Trans. Pattern. Anal. Mach. Intell.*, vol. 29, no. 5, pp. 753–766, May 2007.

[21] C. I. Christodoulou, C. S. Pattichis, M. Pantziaris, and A. Nicolaides, "Texture-based classification of atherosclerotic carotid plaques," *IEEE Trans. Med. Imag.*, vol. 22, no. 7, pp. 902–912, Jul. 2003.

[22] C. Agurto, V. Murray, E. Barriga, S. Murillo, M. S. Pattichis, H. Davis, S. R. Russell, M. D. Abramoff, and P. Soliz, "Multiscale AM-FM methods for diabetic retinopathy lesion detection," *IEEE Trans. Med. Imag.*, vol. 29, no. 2, pp. 502–512, Feb. 2010.

[23] F. Bartolomucci, M. Paterni, C. Morizzo, M. Kozakova, N. D'Allitto, F. Strippoli, C. Palombo, and G. Maiorano, "Early structural changes of carotid artery in familial hypercholesterolemia," *Am. J. Hypertens.*, vol. 14, pp. 125 A–126 A, 2001.

[24] A Philips Medical System Company, "Comparison of image clarity, SonoCT real-time compound imaging versus conventional 2D ultrasound imaging," ATL Ultrasound, Report, ATL Philips Company, Bothell, WA, Sep. 2001.

[25] C. P. Loizou, C. S. Pattichis, M. Pantziaris, T. Tyllis, and A. Nicolaides, "Snakes based segmentation of the common carotid artery intima media," *Med. Bio. Eng. Comput.*, vol. 45, no. 1, pp. 35–49, 2007.

[26] T. Elatrozy, A. N. Nicolaides, T. Tegos, A. Zarka, M. Griffin, and M. Sabetai, "The effect of B-mode ultrasonic image standardization of the echodensity of symptomatic and asymptomatic carotid bifurcation plaque," *Int. Angiol.*, vol. 17, no. 3, pp. 179–186, 1998.

[27] C. P. Loizou, C. S. Pattichis, M. S. Pantziaris, T. Tyllis, and A. N. Nicolaides, "Quantitative quality evaluation of ultrasound imaging in the carotid artery," *Med. Biol. Eng. Comput.*, vol. 44, no. 5, pp. 414–426, 2006.

[28] W. Osika, F. Dangardt, J. Groenros, U. Lundstman, A. Myredall, M. Johansson, R. Volkmann, T. Gustavsson, L. M. Gan, and P. Friberg, "Increasing peripheral artery intima thickness from childhood to seniority," *Arterioscler. Thromb. Vasc. Biol.*, vol. 27, no. 3, pp. 671–676, 2007.

[29] A. Schmidt-Truckass, D. Grathwohl, A. Schmid, R. Boragk, C. Upmeier, J. Keul, and M. Huonker, "Structural, functional, and hemodynamic changes of the common carotid artery with age in male subjects," *Arterioscler. Thromb. Vasc. Biol.*, vol. 19, no. 4, pp. 1091–1097, 1999.

[30] D. J. Williams and M. Shah, "A fast algorithm for active contour and curvature estimation," *GVCIP: Image Underst.*, vol. 55, no. 1, pp. 4–26, 1992.

[31] J. K. Balasundaram and R. S. D. Wahida Banu, "A non-invasive study of alterations of the carotid artery with age using ultrasound images," *Med. Biol. Eng. Comput.*, vol. 44, no. 9, pp. 767–772, 2006.

[32] I. Goncalves, M. W. Lindholm, L. M. Pedro, N. Dias, J. Fernandes, G. N. Fredrikson, J. Nilsson, J. Moses, and M. P. S. Ares, "Elastin and calcium rather than collagen or lipid content are associated with echogenecity of human carotid plaques," *Stroke*, vol. 35, no. 2, pp. 795–800, 2004.

[33] G. Belcaro, A. Barsotti, and A. N. Nicolaides, "Ultrasonic Biopsy: A non-invasive screening technique to evaluate the cardiovascular system and to follow up the progression of atherosclerosis," *Vascular*, vol. 20, pp. 40–50, 1991.

[34] U. Hoffmann, D. Kwait, J. Handwerker, R. Chan, G. Lamuraglia, and T. J. Brady, "Vascular calcification in ex vivo carotid specimens: Precision and accuracy of measurements with multi-detector row CT," *Radiology*, vol. 229, no. 2, pp. 375–381, 2003.

[35] C. P. Loizou, C. S. Pattichis, M. S. Pantziaris, and A. N. Nicolaides, "An integrated system for the segmentation of atherosclerotic carotid plaque," *IEEE Trans. Inform. Techn. Biomed.*, vol. 11, no. 5, pp. 661–667, Nov. 2007.

[36] A. N. Nicolaides, S. K. Kakkos, M. Griffin, M. Sabetai, S. Dhanjil, D. Thomas, G. Geroulakos, N. Georgiou, S. Francis, E. Ioannidou, and C. J. Doré, "Effect of image normalization on carotid plaque classification and the risk of ipsilateral hemispheric events: Results from the asymptomatic carotid stenosis and risk of stroke study," *Vascular*, vol. 1, no. 4, pp. 211–221, 2005.

[37] A. Mojsilovic, M. Popovic, N. Amodaj, R. Babic, and M. Ostojic, "Automatic segmentation of intravascular ultrasound images: A texture based approach," *Annals Biomed. Eng.*, vol. 25, no. 6, pp. 1059–1071, 1997.

[38] M. Budoff and P. Raggi, "Coronary artery disease progression assessed by electron computed tomography," *Am. J. Cardiol.*, vol. 88, no. 2A, pp. 46E–50E, 2001.
[39] J. Budoff, K. Lane, H. Bakhsheshi, S. Mao, B. O. Grassmann, B. C. Friedman, and B. H. Brundage, "Rates of progression of coronary calcium by electron beam tomography," *Am. J. Cardiol.*, vol. 86, no. 1, pp. 8–11, 2000.

C. P. Loizou (M'05) received the B.Sc. degree in electrical engineering and the Dipl.-Ing. (M.Sc.) degree in computer science and telecommunications from the University of Kaisserslautern, Kaisserslautern, Germany, in 1986 and 1990, respectively, and the Ph.D. degree in ultrasound image analysis of the carotid artery from the Department of Computer Science, Kingston University, London, U.K., in 2005.

From 1996 to 2000, he was a Lecturer in the Department of Computer Science, Higher Technical Institute, Nicosia, Cyprus. Since 2000, he has been an Assistant Professor in the Department of Computer Science, School of Sciences and Engineering, Intercollege, Cyprus. He was a Supervisor of a number of Ph.D. and B.Sc. students in the area of computer image analysis and telemedicine. He is also an Associated Researcher at the Institute of Neurology and Genetics, Nicosia, Cyprus. He is the author or coauthor of the book *Despeckle Filtering Algorithms and Software for Ultrasound Imaging*, 12 chapters in books, 13 referred journals, and 52 conference papers in the fields of image and video analysis. His research interests include medical imaging and processing, motion and video analysis, signal and image processing, pattern recognition, biosignal analysis, in ultrasound, magnetic resonance, and optical coherence tomography imaging and computer applications in medicine.

Dr. Loizou is a Senior Member of the Institution of Electrical Engineers.

V. Murray (M'01) received the B.S. (high honors – ranked first in class) degree in electrical engineering from the Pontificia Universidad Católica del Perú, Lima, Perú, in 2003, and the M.S. and Ph.D. degrees in electrical engineering from the University of New Mexico (UNM), Albuquerque, in 2005 and 2008, respectively.

He is currently a Research Assistant Professor in the Department of Electrical and Computer Engineering, UNM, where he is developing adaptive reconfigurable hardware, based on FPGAs, for the Air Force Research Laboratory and developing methods and algorithms in medical imaging for detecting diseases in human eyes for VisionQuest Biomedical, Albuquerque. His research interests include amplitude modulation-frequency modulation demodulation methods, digital image and video processing, medical imaging, and hardware design using very high descriptive language (VHDL) and field programmable gate arrays (FPGAs).

M. S. Pattichis (M'99–SM'06) received the B.Sc. (high honors and special honors) degree in computer sciences and the B.A. (high honors) degree in mathematics, the M.S. degree in electrical engineering, and the Ph.D. in computer engineering, in 1991, 1993, and1998, respectively, all from the University of Texas at Austin, Austin.

He is currently an Associate Professor in the Department of Electrical and Computer Engineering, University of New Mexico (UNM), Albuquerque, where he is also an Associate Professor in the Department of Radiology. He is an Associate Editor of the Pattern Recognition. His research interests include digital image, and video processing and communications, dynamically reconfigurable computer architectures, and biomedical and space-image-processing applications.

Dr. Pattichis is an Associate Editor of the IEEE TRANSACTIONS ON INDUSTRIAL INFORMATICS. He was the General Chair of the 2008 IEEE Southwest Symposium on image analysis and interpretation. He was a recipient of the 2004 Electrical and Computer Engineering Distinguished Teaching Award, and the 2006 School of Engineering Harrison Faculty Recognition Award at UNM.

M. Pantziaris received the M.D. degree in neurology from the Aristotelion University, Thessaloniki, Greece, in 1995.

He is currently a Senior Neurologist in the Neurological Department, Cyprus Institute of Neurology and Genetics, Nicosia, Cyprus, and is also the Head of the Neurovascular Department. He was trained in Carotid Duplex–Doppler ultrasonography at St. Mary's Hospital, London, in 1995. In 1999, he was a Visiting Doctor in acute stroke treatment at Massachusetts General Hospital, Harvard University, Boston. He has considerable experience in carotid–transcranial ultrasound, has participated in many research projects, and has several publications to his name. He is also the head of the Multiple Sclerosis (MS) Clinic, where he is running research projects studying the etiology and therapy of MS.

C. S. Pattichis (S'88–M'88–SM'99) was born in Cyprus on January 30, 1959. He received the Diploma degree in technician engineering from the Higher Technical Institute, Nicosia, Cyprus, in 1979, the B.Sc. degree in electrical engineering from the University of New Brunswick, New Brunswick, Canada, in 1983, the M.Sc. degree in biomedical engineering from the University of Texas at Austin, Austin, in 1984, the M. Sc. degree in neurology from the University of Newcastle Upon Tyne, U.K., in 1991, and the Ph.D. degree in electronic engineering from the University of London, London, U.K., in 1992.

He is currently a Professor in the Department of Computer Science, University of Cyprus, Nicosia. His research interests include e-health, medical imaging, biosignal analysis, and intelligent systems. He has been involved in numerous projects in these areas funded by EU, the National Research Foundation of Cyprus, the INTERREG, and other bodies, with a total funding managed in excess of 5 million Euros. He was on the Editorial Board of the *Journal of Biomedical Signal Processing and Control*. He is the Coeditor of the books: *M-Health: Emerging Mobile Health Systems* (New York: Springer, 2006), and *Information Technology in Biomedicine* (IEEE, to be published in 2010). He is the coauthor of the monograph *Despeckle Filtering Algorithms and Software for Ultrasound Imaging* (San Rafael, CA: Morgan & Claypool, 2008). He is the author or coauthor of 52 refereed journal and 142 conference papers, and 19 chapters in books in these areas.